Three-dimensional model of electrostatically induced pattern formation in thin polymer films

Dongchoul Kim and Wei Lu*
Department of Mechanical Engineering, University of Michigan, Ann Arbor, Michigan 48109, USA
(Received 12 October 2005; published 10 January 2006)

Experiments have shown that a thin polymer film subjected to an electrostatic field may lose stability at the polymer-air interface, leading to uniform self-organized pillars emerging out of the film surface. This paper presents a three-dimensional model to account for this behavior. Attention is focused on a fully nonlinear evolution simulation to reveal the dynamic process from an early perturbation to late structure formation. Energetic components involving the interface energy and dielectric effect and the kinetics of coupled viscous flow and diffusion are incorporated into a phase field framework. The semi-implicit Fourier spectral method and preconditioned biconjugate-gradient method are applied for high efficiency and numerical stability. The simulations reveal rich dynamics of the pattern formation process, and show that the kinetic constraint of the substrate can essentially limit structure coarsening. The pillar size is insensitive to the film thickness while the distance between pillars and the growth rate are significantly affected. The study also suggests an approach to control structural formation in thin films with a designed electric field.

DOI: 10.1103/PhysRevB.73.035206 PACS number(s): 61.25.Hq, 68.35.Md, 64.70.Nd

I. INTRODUCTION

Controlled formation of organized structures in thin polymer films has significant applications. Emerging technologies in polymer-based semiconductors and functional devices, such as polymer light-emitting diodes (LEDs),[1,2] printed integrated circuits,[3] and inexpensive solar cells,[4] rely on the production of features of increasingly smaller dimensions. Recent experiments show that an electric field may induce self-organized morphological patterns, suggesting a potential low-cost and high-throughput approach for nanofabrication.[5–9] In the process, a polymer thin film was first spin coated on a substrate. The film was then heated to above its glass transition temperature. An electric field was applied to the polymer melt, which destabilized the flat polymer-air interface and led to the formation of uniform pillars emerging out of the film. In addition to the technical importance, the discoveries pose interesting scientific problems. The major issues are the mechanism by which an interface loses its stability, and how the instability leads to the final pattern of quite uniform pillars. This paper aims to address these questions and reveal the dynamic self-organization process. A three-dimensional simulation is made viable via a phase field model and an efficient numerical approach.

The phenomenon that an interface loses its stability in an electrostatic field is also known as electrohydrodynamic instability. From the energetic point of view, the behavior can be explained in terms of two competing actions: surface energy and electrostatic energy.[10] Under the condition of lubrication approximation of a viscous flow, linear or weakly nonlinear perturbation analyses have been performed.[11–13] These studies point out that a wavy interface reduces the electrostatic energy, but increases the interface energy. The competition determines a critical wavelength. A perturbation with a larger wavelength will grow over time. The fastest-growth wavelength is related to the field strength such that a stronger electric field leads to a smaller wavelength. The lubrication approximation fails in situations of small surface tension and large electric field. However, such situations are typical to generate small pillar arrays. Pease and Russel recently proposed a more general linear stability analysis without the constraint of the lubrication approximation.[14]

While stability analysis provides valuable insight into the early stage evolution, it is still not clear how the instability leads to the final pattern. This would require a reliable and accurate explanation of the thin film behavior in the nonlinear evolution regime. For a thin film, the self-assembly process is significantly affected by the substrate. The fast-growth wavelength obtained from small-perturbation analysis may not have sufficient time to develop before it meets the substrate, and thus has no direct connection to the size of the late structure. The lack of a kinetic route may essentially prevent the coarsening of pillars when the film breaks. When the film thickness is comparable to or smaller than the fast wavelength, even the early evolution is considerably affected by the substrate. In addition, experiments have shown notable diffusion in thin polymer films,[15–17] which needs to be considered to provide more accurate prognostications. A careful consideration of the problem leads us to the point that the phenomenon may have a complex nature and involve rich dynamics.

This paper proposes a three-dimensional dynamic model to reveal a detailed picture of the small-size morphology evolution process. We consider energetic components involving the interface energy and dielectric effect, and the kinetics of coupled viscous flow and diffusion. The evolving interfaces and multiple energetics and kinetics pose a computational challenge. This is addressed by modeling the system with a diffuse interface framework, where an interface is represented by a thin continuous transition region. We have applied a similar approach to study interface diffusion problems in several material systems.[18–21] The diffuse interface concept has also been used for polymer blends.[22,23] In contrast to interface tracking methods such as boundary element methods, the interfaces are not modeled explicitly but given implicitly by the concentration field. Consequently, complex changes will not cause any additional computational diffi-

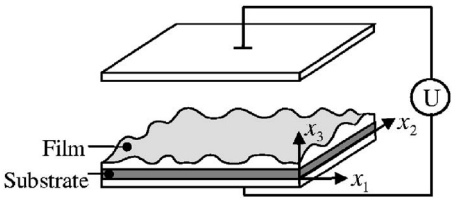

FIG. 1. Illustration of a thin polymer film on a substrate subjected to an electrostatic field. The field is generated by two electrodes parallel to the film, one above the polymer surface and the other underneath the substrate.

culty. Phenomena such as a film breaking into isolated islands or a pillar bridging two electrodes can be captured naturally. To achieve high efficiency and numerical stability, we apply the semi-implicit Fourier spectral method and preconditioned biconjugate-gradient method. The following is the plan of this paper. Section II develops the model. The numerical approach is discussed in Sec. III. Representative results are given in Sec. IV. Section V is the summary.

II. A DIFFUSE INTERFACE MODEL

Figure 1 shows a thin polymer film on a substrate subjected to an electrostatic field. The field is generated by two electrodes parallel to the film, one above the polymer surface and the other underneath the substrate. The system is infinitely large in the lateral direction. When heated, the polymer film may change its morphology via diffusion and viscous flow. The substrate does not evolve. A coordinate system is attached so that the x_1-x_2 plane coincides with the bottom of the substrate. Define a concentration c by the volume fraction of polymer, $c=0$ for pure air phase and $c=1$ for pure polymer phase. Regard the concentration as a spatially continuous and time-dependent function $c(x_1,x_2,x_3,t)$.

The free energy of the system depends on the phase configuration and electric field distribution, namely,

$$G=\int_V \left(f(c)+\frac{1}{2}h|\nabla c|^2-\frac{1}{2}\varepsilon_0\varepsilon_r(c)|\nabla\phi|^2\right)dV. \tag{1}$$

The integration extends over the entire volume between the two electrodes. The $f(c)$ term represents the chemical energy, which drives phase separation. We use a double-well function $f(c)=f_0c^2(c-1)^2$, where f_0 is a positive constant. The function has two minima corresponding to the polymer and air phases, respectively. The second term accounts for the interface energy between polymer and air, where h is a material constant. The first two terms are typical in the Cahn-Hilliard model.[24] The third term represents the electrostatic energy, where ϕ is the electric potential, $\varepsilon_0=8.85\times10^{-12}$ F/m is the vacuum permittivity, and ε_r is the dielectric constant of the medium.[25] The dielectric constant may be interpolated linearly from those of the polymer and air, namely, $\varepsilon_r(c)=\varepsilon_r^{polymer}c+\varepsilon_r^{air}(1-c)$. The specific form is insignificant when the interface region is thin. Similar linear interpolation has also been used for other properties, such as elastic constants[26] and surface stress.[27,28] Note that the volume integration in Eq. (1) includes the substrate, since its electric field is affected by the morphology change of the film. In the substrate region, the first two terms in Eq. (1) are irrelevant. It is only necessary to let $\varepsilon_r(c)=\varepsilon_r^{substrate}$ and calculate the third term. For computational convenience, we may treat the substrate as a special part of the film, which does not evolve, keeps constant $c=1$, and has the property of $\varepsilon_r^{substrate}$. Thus Eq. (1) also applies to the substrate region since the first two terms disappear automatically. In this way the film and substrate can be treated uniformly. We consider situations that the film wets the substrate to keep their interface intact, i.e., no substrate exposure during evolution. Hence Eq. (1) excludes the nonvarying film-substrate interface energy.

When there is no free charge in the dielectric medium, the electric potential satisfies

$$\nabla\cdot(\varepsilon_r\nabla\phi)=0. \tag{2}$$

This equation combined with the appropriate boundary conditions gives the electrostatic field for any given concentration distribution.

The chemical potential is defined by $\mu=\delta G/\delta c$. When diffusion is the only mass transport mechanism, the diffusion flux is given by $\mathbf{J}=-M\nabla\mu$, where M is the mobility. Viscous flow adds a convection term to the flux. Denote the flow velocity by $\mathbf{v}$. The convection flux is given by $c\mathbf{v}$. Note that the film morphology is limited by slow polymer flow. The air flow can be neglected, i.e., treated as vacuum. We will consider incompressible flow so that $\nabla\cdot\mathbf{v}=0$. In the concurrent kinetic process, the net flux is the sum of the diffusion flux and the convection flux. This, combined with the mass conservation relation $\partial c/\partial t+\nabla\cdot\mathbf{J}=0$, gives a convective Cahn-Hilliard equation, namely,

$$\frac{\partial c}{\partial t}+\mathbf{v}\cdot\nabla c=\nabla\cdot(M\nabla\mu). \tag{3}$$

With the presence of a diffuse interface, the modified Navier-Stokes equation describes the viscous flow[29]

$$\rho\left(\frac{\partial\mathbf{v}}{\partial t}+\mathbf{v}\cdot\nabla\mathbf{v}\right)=-\nabla p+\nabla\cdot(\eta\nabla\mathbf{v})+\mu\nabla c. \tag{4}$$

Here ρ is the density, η the viscosity, and p the pressure that enforces the incompressibility constraint $\nabla\cdot\mathbf{v}=0$. The term $\mu\nabla c$ accounts for the force at the interface. We normalize the governing equations with a characteristic velocity V_c, length L_c, and time $t_c=L_c/V_c$. The choice of the magnitudes of the characteristic quantities depends on the physical detail to resolve and computational convenience. Equation (2) retains the same form after normalization. Other dimensionless equations are

$$\frac{\partial c}{\partial t}+\mathbf{v}\cdot\nabla c=\frac{1}{\mathrm{Pe}}\nabla\cdot(M\nabla\mu), \tag{5}$$

$$\mu=4c^3-6c^2+2c-\mathrm{Ch}^2\nabla^2c-\frac{1}{2}(\Delta\varepsilon_r)|\nabla\phi|^2, \tag{6}$$

$$-\nabla p+\nabla\cdot(\eta\nabla\mathbf{v})+\frac{1}{\mathrm{Ca}}\mu\nabla c=0. \tag{7}$$

The mobility M and viscosity η are dimensionless numbers normalized by those of the polymer, M_0 and η_0. We will consider position-dependent M and η, as discussed later. The potential field ϕ is normalized by $\phi_c = L_c\sqrt{f_0/\varepsilon_0}$. Here we have $\Delta\varepsilon_r = \varepsilon_r^{polymer} - \varepsilon_r^{air}$ in the region above the substrate, and $\Delta\varepsilon_r = \varepsilon_r^{substrate} - \varepsilon_r^{air}$ in the substrate. The Péclet number $\mathrm{Pe} = V_c L_c/(M_0 f_0)$ reflects the ratio of the diffusive time scale and the convective time scale. The significance of the interface energy is described by the Cahn number $\mathrm{Ch} = \sqrt{h/f_0}/L_c$. The Reynolds number $\mathrm{Re} = \rho V_c L_c/\eta_0$ reflects the ratio of inertial and viscous forces. We consider a viscous polymer fluid at moderate velocities, i.e., low Reynolds number. Equation (7) has neglected the inertia term, i.e., the left-hand side of Eq. (4). Thus the velocity is instantaneously inferrable from the concentration. The capillary number $\mathrm{Ca} = \eta_0 V_c/(L_c f_0)$ affects the relative magnitude of viscous force and interface force.

III. NUMERICAL IMPLEMENTATION

Equations (2) and (5)–(7) need to be solved simultaneously to obtain the evolution sequence. The numerical approach needs to have a high spatial resolution to resolve the high-order derivatives in the diffusion equation as well as the large gradients at the interface region. The approach should also be efficient and stable for the time integration, which is especially important for three-dimensional simulations. We propose an efficient semi-implicit Fourier spectral method for both high spatial resolution and fast computation. The central idea of the semi-implicit method is to treat the linear term implicitly and the nonlinear term explicitly to allow for larger time steps without losing numerical stability.[30,31] In contrast, a fully implicit treatment yields expensive schemes while explicit discretization quickly leads to numerical instability or needs impractical time-step constraint.

We choose the space between the two electrodes as a calculation domain. The substrate and the polymer film are treated uniformly to avoid the need to explicitly prescribe the flow and diffusion boundary condition at the substrate surface. The uniform treatment also enables the application of the efficient spectral method in three dimensions. We consider the substrate as part of the film, but ensure by kinetics that this part does not flow or diffuse. In other words, we assign $M=0$ and $\eta \gg 1$ in the substrate region so that it keeps $c=1$. Above the substrate, according to the normalization, we have $M=1$ and $\eta=1$. This leads to position-dependent M and η in Eqs. (5) and (7).

To consider variable mobility, we rewrite the right-hand side of Eq. (5) as

$$\nabla \cdot (M \nabla \mu) = A \nabla^2 \mu_{lr} + s_\mu, \tag{8}$$

where A is a constant, μ_{lr} a linear component of μ, and $s_\mu = \nabla \cdot (M \nabla \mu) - A \nabla^2 \mu_{lr}$. The idea is to treat the linear term $A\nabla^2\mu_{lr}$ implicitly and treat the s_μ term explicitly. This semi-implicit approach can significantly alleviate the time-step constraint. The convective term $\mathbf{v}\cdot\nabla c$ is treated explicitly. There are different choices for μ_{lr}.[31–33] We have obtained numerical stability in all our simulations by taking $\mu_{lr} = c - \mathrm{Ch}^2\nabla^2 c$ and $A=1$. Note that the stability is achieved in conjunction with the extrapolated Gear (SBDF) scheme for time integration. Among the second-order multistep methods, SBDF has the strongest high-modal decay.[33] This provides the required damping for the very high frequencies in the diffusion equation without a harsh time-step constraint. Applying the scheme to the normalized diffusion equation (5), we obtain the following discretized form:

$$\frac{3}{2}c^{n+1} - 2c^n + \frac{1}{2}c^{n-1} = \frac{A\Delta t}{\mathrm{Pe}}(\nabla^2 c^{n+1} - \mathrm{Ch}^2\nabla^4 c^{n+1}) + 2Q^n - Q^{n-1}, \tag{9}$$

where

$$Q^n = \frac{\Delta t}{\mathrm{Pe}}(\nabla \cdot M \nabla \mu^n - A\nabla^2 c^n + A\mathrm{Ch}^2\nabla^4 c^n) - \Delta t \mathbf{v}^n \cdot \nabla c^n. \tag{10}$$

Equation (9) can be solved efficiently in the Fourier space. Applying the Fourier transform to Eqs. (9) and (10), we obtain

$$\hat{c}^{n+1} = \frac{4\hat{c}^n - \hat{c}^{n-1} + 4\hat{Q}^n - 2\hat{Q}^{n-1}}{3 + (2A\Delta t/\mathrm{Pe})(k^2 + \mathrm{Ch}^2 k^4)}, \tag{11}$$

$$\hat{Q}^n = \frac{\Delta t}{\mathrm{Pe}}\{i\mathbf{k}\cdot[M(i\mathbf{k}\hat{\mu}^n)_\mathbf{r}]_\mathbf{k} + Ak^2\hat{c}^n + Ak^4\mathrm{Ch}^2\hat{c}^n\} - \Delta t[\mathbf{v}^n \cdot (i\mathbf{k}\hat{c}^n)_\mathbf{r}]_\mathbf{k}, \tag{12}$$

where the caret and the subscript $\mathbf{k}$ stand for the Fourier transform. The vector $\mathbf{k}$ denotes the wave vector in Fourier space, and $k^2 = k_1^2 + k_2^2 + k_3^2$. The subscript $\mathbf{r}$ denotes the inverse Fourier transform.

The velocity field is solved by Eq. (7) and the incompressibility condition. To treat the variable viscosity, we rewrite

$$\nabla \cdot (\eta \nabla \mathbf{v}) = B\nabla^2 \mathbf{v} + \mathbf{r}(\mathbf{v}), \tag{13}$$

where $\mathbf{r}(\mathbf{v}) = \nabla\cdot(\eta\nabla\mathbf{v}) - B\nabla^2\mathbf{v}$ and B is a constant. We take $B = \max(\eta)$ in our simulations, and have achieved numerical stability in all situations. Taking the divergence on both sides of Eq. (7) and applying the incompressibility constraint $\nabla\cdot\mathbf{v}=0$, we obtain the pressure at the nth time step

$$\nabla^2 p^n = \nabla \cdot \mathbf{r}(\mathbf{v}^{n-1}) + \frac{1}{\mathrm{Ca}}\nabla\cdot(\mu^n \nabla c^n). \tag{14}$$

The velocity field is given by reorganizing Eq. (7), namely,

$$\nabla^2 \mathbf{v}^n = \frac{1}{B}\left(\nabla p^n - \mathbf{r}(\mathbf{v}^{n-1}) - \frac{1}{\mathrm{Ca}}(\mu^n \nabla c^n)\right). \tag{15}$$

The corresponding equations in Fourier space are given by

$$\hat{p}^n = -\frac{1}{k^2}\left(i\mathbf{k}\cdot\hat{\mathbf{r}}(\mathbf{v}^{n-1}) + \frac{1}{\mathrm{Ca}} i\mathbf{k}\cdot[\mu^n (i\mathbf{k}\hat{c}^n)_\mathbf{r}]_\mathbf{k}\right), \tag{16}$$

$$\hat{\mathbf{v}}^n = -\frac{1}{Bk^2}\left(i\mathbf{k}\hat{p}^n - \hat{\mathbf{r}}(\mathbf{v}^{n-1}) - \frac{1}{\mathrm{Ca}}[\mu^n (i\mathbf{k}\hat{c}^n)_\mathbf{r}]_\mathbf{k}\right). \tag{17}$$

Equations (16) and (17) are solved iteratively.

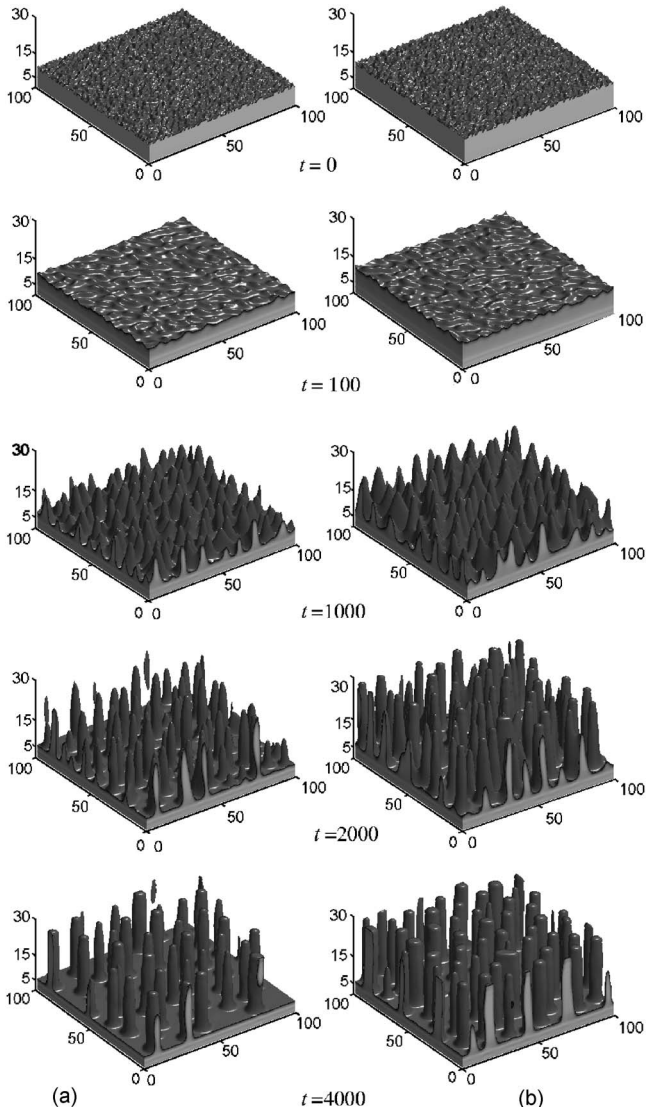

FIG. 2. Comparison of two evolution sequences. The film is subjected to a normalized voltage of $U=22$ between the two electrodes. The film thickness is 3.5 in (a) and 5.5 in (b).

The electric field is determined by Eq. (2), which can also be written as $\varepsilon_r \nabla^2 \phi + \nabla \varepsilon_r \cdot \nabla \phi = 0$. We apply the second-order discretization and compute the matrix with the preconditioned biconjugate-gradient method.[34] The Jacobi preconditioner is adopted. The approach allows efficient computation of large three-dimensional (3D) domains.

In the following we outline the procedure to compute c^{n+1} from c^n. First compute the electric potential field ϕ^n that corresponds to the concentration distribution c^n. Then substitute the solution of ϕ^n into Eq. (6) to get μ^n. Solving the modified Navier-Stokes equation in Fourier space by Eqs. (16) and (17) gives $\hat{p}^n$ and $\hat{\mathbf{v}}^n$. Using $\hat{c}^n$, $\hat{\phi}^n$, and $\hat{\mathbf{v}}^n$, we compute the convective Cahn-Hilliard equation in Fourier space by Eqs. (11) and (12) to obtain $\hat{c}^{n+1}$. The new concentration c^{n+1} is obtained from $\hat{c}^{n+1}$ by the inverse Fourier transform. The procedure is repeated until a prescribed time.

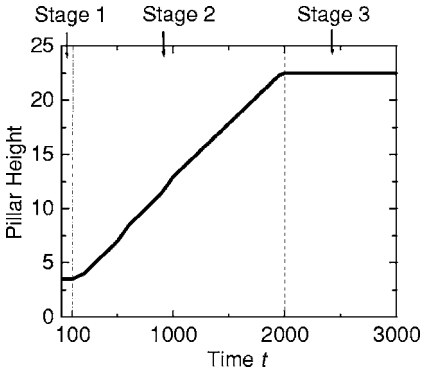

FIG. 3. Three growth stages in the evolution process.

IV. NUMERICAL RESULTS

A series of simulations have been performed, which give a whole picture of the self-organization process. Representative results are shown in Figs. 2–7. The 3D figures show the snapshots of the polymer surface at chosen time steps. The surface is defined by the 0.5 concentration. We use a domain size of $100 \times 100 \times 30$ in all the simulations. The substrate has a thickness of 5. Assigning $M=0$ and $\eta=500$ in the substrate region is sufficient to keep it unchanged. The simulations start from random initial conditions, i.e., flat films with small random perturbations. Without any applied electric field, the simulations show that an initial perturbation quickly dies away. The polymer film becomes flat to minimize the surface energy. In contrast, an applied electric field leads to surface instability and rich dynamics.

Figure 2 shows a comparison of two evolution sequences from $t=0$ to 4000. The film is subjected to a normalized voltage of $U=22$ between the two electrodes. This voltage produces an electric field strength of 10^7-10^8 V/m, which is typical in experiments. The two sequences are different in

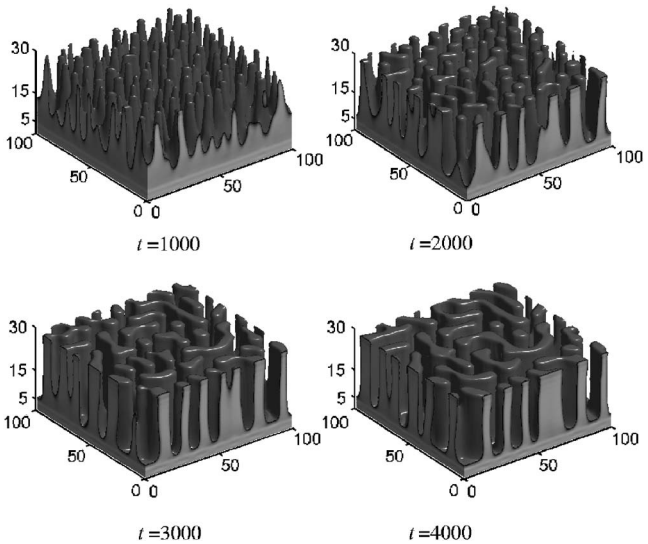

FIG. 4. Evolution sequence for a relatively thick film with a thickness of 10.5. The film continues to evolve after touching the ceiling, leading to significant coarsening. This changes the pillar structure into an interwoven stripe structure.

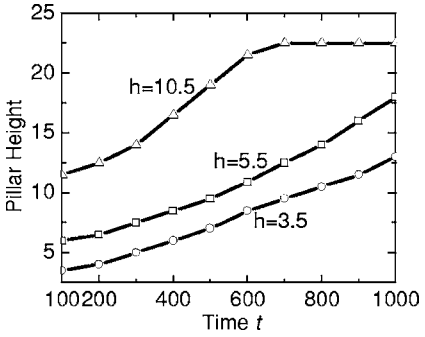

FIG. 5. Pillar height as a function of time for different initial film thickness h. A thicker film demonstrates substantially higher growth rate due to less constraint by the substrate.

the initial film thickness, which is 3.5 in (a) and 5.5 in (b). We use the same material parameters in the simulations. The Péclet number is taken to be Pe=10, which is representative of real polymers under relatively weak shearing conditions. The Cahn number and the capillary number are taken to be Ch=0.5 and Ca=10, respectively. The dielectric constant of air is $\varepsilon_r^{air}=1$. The dielectric constant for the polymer film (polyethylene) is $\varepsilon_r^{polymer}=2.25$. We also assign $\varepsilon_r^{substrate}=2.25$ for the substrate. The two sequences in Fig. 2 demonstrate similar characteristic behaviors. When the electrostatic field is applied, the surface undulation grows over time. Ripples with small amplitude and wavelength emerge at about $t=100$. The interwoven ripples have different orientations and lengths, but their widths are similar, suggesting a representative size scale. During the growth, longer ripples break into shorter ones. At $t=1000$, the ripples become small cones as the electrostatic energy overcomes the surface energy and pulls the interface further upward. The cones have a size scale larger than the ripples, suggesting a concurrent growth in the lateral and vertical directions. They are densely packed with the bases in contact, and the distance between two neighboring cones is comparable to their size. The cones

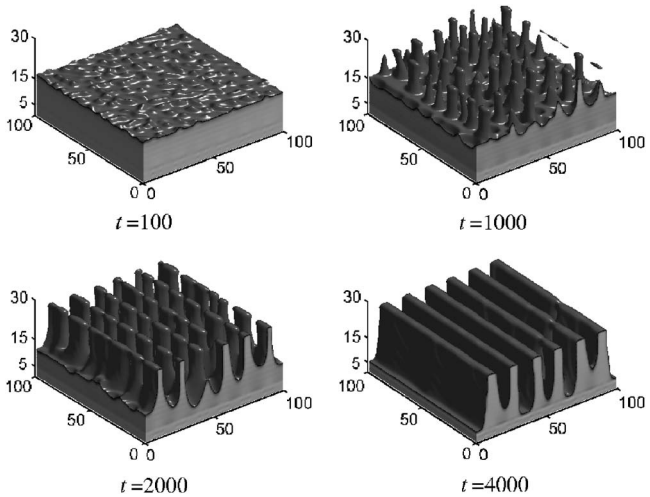

FIG. 6. Evolution sequence with patterned electrodes. The film has a thickness of 10.5. After touching the ceiling, the narrow pillars coarsen and merge into a stripe pattern replicating the electrodes.

continue to grow and evolve into pillars. After that, growth is only observed in the vertical direction and the pillars maintain a stable size. The pillars grow higher by absorbing the surrounding material. Eventually, the film thickness between pillars becomes so thin that the kinetic constraint of the substrate essentially stops any subsequent coarsening and growth, though the lateral coarsening of pillars can further reduce the electrostatic energy. The film evolves into quite uniform pillars at $t=4000$. The comparison between the two sequences of (a) and (b) indicates that a thicker film grows faster. The pillar size is insensitive to the film thickness. However, the interpillar distance is significantly affected. A thicker film produces a more densely packed morphology.

The simulations reveal that the pillar size is determined during the evolution process. Energetics by itself cannot select the final structure. This suggests an experimental investigation of the kinetic process. It is also shown that the morphological evolution of the film is fundamentally different from crystal growth. The latter is limited by the kinetic process at the growth front, such as phase transition or diffusion. However, the pillar growth is limited by the kinetic process at the base, where the mass accumulation pushes the entire pillar higher. It should be emphasized that the mechanism of pillar growth is not mass transport from the base to the top. Instead, a pillar grows higher by continuously forming new bases with the absorbed material. Thus the process involves only local mass transport, and a pillar maintains its morphology during growth until it is close to the top electrode. The pillar front may then change its shape due to the variation of the electric field or touching the electrode. From a kinetics point of view, the morphology change from ripples to pillars represents a transition from front kinetics to base kinetics.

Tracking the height change of a pillar provides quantitative information about its growth. Figure 3 shows the curve of pillar height as a function of time for the film in Fig. 2(a), which has an initial thickness of 3.5. The pillars have a quite narrow height distribution. To be definite, we choose a representative pillar close to the center and measure its height from the top to the substrate surface. Three stages can be identified in Fig. 3, which are consistent with experimental observations.[35,36] The first stage is characterized by slow dynamics: the undulation does not show any significant increase until $t=100$. After that, ripples with small amplitude and wavelength start to emerge and quickly grow into pillars. This second stage is characterized by significant height change. If the two electrodes are close enough, the pillars may reach the top electrode and flat their fronts: this is the third stage. When the film is thick, considerable lateral coarsening can happen due to the available kinetic route for mass transport. Figure 4 shows the sequence for a film of thickness 10.5. The dense pillars begin to touch the ceiling at about $t=1000$. Further lateral growth leads to a serpentine structure. Figure 5 shows the dependence of growth rate on film thicknesses between $t=100$ and 1000. This is the time frame that significant height growth happens. A thicker film demonstrates substantially higher growth rates due to less constraint from the substrate. The multiple growth regimes suggest that the growth process may not be fitted meaningfully by a single phenomenological relationship. However, for a particular regime, it may be possible to describe the pillar height

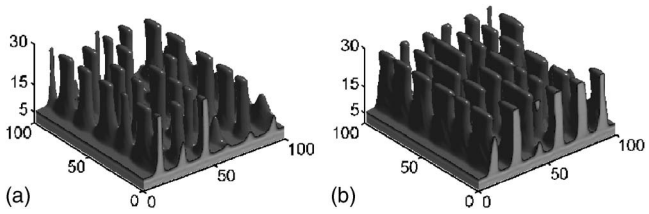

FIG. 7. Structures at $t=4000$ induced by patterned electrodes. The film has a thickness of 3.5 in (a) and 5.5 in (b). The lack of material and the kinetic constraint prevent the formation of continuous stripes.

h in terms of a power law $h \sim t^n$. For the regime in Fig. 5, curve fitting seems to suggest a trend from $h \sim t$ to $h \sim t^2$ when the film becomes thicker.

To investigate the effect of designed electric fields, we have performed simulations with patterned electrodes. The electrode consists of six stripes, each having a width of 5. The same normalized voltage of $U=22$ is applied. Figure 6 shows the result for a film thickness of 10.5. The width of the electrode is smaller than the diameter of a pillar, which changes the cross section from circular to elliptical. The pillars emerge to orientate along the electrode. After touching the ceiling, the narrow pillars coarsen and merge. This leads to a stripe pattern replicating the patterned electrodes. Figure 7 shows that thinner films form aligned pillars. The lack of material and the kinetic constraint prevent the formation of continuous stripes, so that the film stops at a morphology similar to that in Fig. 6 at $t=2000$. These simulations suggest a significant degree of experimental control in directing thin film morphologies with a designed electric field.

V. CONCLUSIONS

Experiments have shown that the polymer-air interface instability in an electrostatic field may lead to the formation of organized pillar arrays. The dynamic process between the early perturbation and late structure formation is crucial to understand such a self-assembly behavior. A phase field model is proposed in this paper, which incorporates viscous flow, diffusion, and the dielectric mechanism. The coupled system is numerically solved by the semi-implicit Fourier spectral method and the preconditioned biconjugate-gradient method. The 3D simulations reveal the dynamic evolution process in the nonlinear regime. The competition between the electrostatic energy and the surface energy leads to a characteristic pillar size. This length scale is not determined by energy minimization, but by an interplay between the energetics and kinetics. The film thickness significantly influences the growth rate and the distance between pillars. A thinner film evolves more slowly due the substrate constraint. The simulations have shown that a thicker film leads to denser pillar arrays, and the cylindrical pillars may transform into stripes after they bridge the two electrodes. This demonstrates an approach to morphology control via kinetic constraints. With patterned electrodes, we have obtained parallel stripes replicating the electrode pattern. A very thin film, however, produces narrow elliptic pillars along the electrodes. These simulations suggest a significant degree of experimental control in directing thin film morphologies with a designed electric field.

ACKNOWLEDGMENT

The authors acknowledge financial support from National Science Foundation Career Award No. DMI-0348375.

*Corresponding author. FAX: (734)647-3170. Email address: weilu@umich.edu

[1] D. Braun, Mater. Today **5** (6), 32 (2002).
[2] K. Tada, Thin Solid Films **417**, 32 (2002).
[3] C. J. Drury, C. M. J. Mutsaers, C. M. Hart, M. Matters, and D. M. d. Leeuw, Appl. Phys. Lett. **73**, 108 (1998).
[4] N. S. Sariciftci, Curr. Opin. Solid State Mater. Sci. **4**, 373 (1999).
[5] E. Schäffer, T. Thurn-Albrecht, and T. P. Russell, Nature (London) **403**, 874 (2000).
[6] M. D. Morariu, N. E. Voicu, E. Schäffer, Z. Lin, T. P. Russell, and U. Steiner, Nat. Mater. **2**, 48 (2003).
[7] D. Salac, W. Lu, C. W. Wang, and A. M. Sastry, Appl. Phys. Lett. **85**, 1161 (2004).
[8] S. Y. Chou and L. Zhuang, J. Vac. Sci. Technol. B **17**, 3197 (1999).
[9] S. Y. Chou, L. Zhuang, and L. J. Guo, Appl. Phys. Lett. **75**, 1004 (1999).
[10] Z. Suo and J. Liang, Appl. Phys. Lett. **78**, 3971 (2001).
[11] E. Schäffer, T. Thurn-Albrecht, T. P. Russell, and U. Steiner, Europhys. Lett. **53**, 518 (2001).
[12] L. Wu and S. Y. Chou, Appl. Phys. Lett. **82**, 3200 (2003).
[13] Z. Lin, T. Kerle, S. M. Baker, D. A. Hoagland, E. Schäffer, U. Steiner, and T. P. Russell, J. Chem. Phys. **114**, 2377 (2001).
[14] L. F. Pease III and W. B. Russel, J. Chem. Phys. **118**, 3790 (2003).
[15] M. F. Toney, T. P. Russell, J. A. Logan, H. Kikuchi, J. M. Sands, and S. K. Kumar, Nature (London) **374**, 709 (1995).
[16] B. Frank, A. P. Gast, T. P. Russell, H. R. Brown, and C. Hawker, Macromolecules **29**, 6531 (1996).
[17] X. Zheng, M. H. Rafailovich, J. Sokolov, Y. Strzhemechny, S. A. Schwarz, B. B. Sauer, and M. Rubinstein, Phys. Rev. Lett. **79**, 241 (1997).
[18] W. Lu and D. Kim, Nano Lett. **4**, 313 (2004).
[19] W. Lu and D. Salac, Phys. Rev. Lett. **94**, 146103 (2005).
[20] K. S. Schneider, W. Lu, T. M. Owens, D. R. Fosnacht, M. M. Banaszak Holl, and B. G. Orr, Phys. Rev. Lett. **93**, 166104 (2004).
[21] D. Kim and W. Lu, Nanotechnology **15**, 667 (2004).
[22] B. J. Keestra, P. C. J. V. Puyvelde, P. D. Anderson, and H. E. H. Meijer, Phys. Fluids **15**, 2567 (2003).
[23] T. Roths, C. Friedrich, M. Marth, and J. Honerkamp, Rheol. Acta **41**, 211 (2002).
[24] J. W. Cahn and J. E. Hilliard, J. Chem. Phys. **28**, 258 (1958).
[25] L. D. Landau and E. M. Lifshitz, *Electrodynamics of Continuous*

Media (Pergamon Press, New York, 1984).
[26] S. Y. Hu and L. Q. Chen, Acta Mater. **49**, 1879 (2001).
[27] W. Lu and Z. Suo, Phys. Rev. B **65**, 085401 (2002).
[28] W. Lu and Z. Suo, Phys. Rev. B **65**, 205418 (2002).
[29] M. E. Gurtin, D. Polignone, and J. Viñals, Math. Models Meth. Appl. Sci. **6**, 815 (1996).
[30] W. Lu and Z. Suo, J. Mech. Phys. Solids **49**, 1937 (2001).
[31] J. Zhu, L.-Q. Chen, J. Shen, and V. Tikare, Phys. Rev. E **60**, 3564 (1999).
[32] J. J. Douglas and T. Dupont, *Numerical Solution of Partial Differential Equations* (Academic Press, New York, 1971).
[33] U. M. Ascher, S. J. Ruuth, and B. T. R. Wetton, SIAM (Soc. Ind. Appl. Math.) J. Numer. Anal. **32**, 797 (1995).
[34] G. H. Golub and C. F. V. Loan, *Matrix Computation* (Johns Hopkins University Press, Baltimore, 1989).
[35] P. Deshpande, X. Sun, and S. Y. Chou, Appl. Phys. Lett. **79**, 1688 (2001).
[36] Z. Lin, T. Kerle, T. P. Russell, E. Schäffer, and U. Steiner, Macromolecules **35**, 3971 (2002).